

<https://doi.org/10.1038/s43247-024-01732-w>

Rapid response of stream dissolved phosphorus concentrations to wildfire smoke

**Nicole M. Fernandez** , **Hunter T. Jamison** & **Zoë Gold**

Wildfires can produce large plumes of smoke that are transported across vast distances, altering nutrient cycling of undisturbed watersheds exposed downwind. To date, wildfire smoke influence on stream biogeochemical signatures remains an important knowledge gap. Here we evaluate the impacts of wildfire smoke on phosphorus (P) biogeochemical cycling in a temperate watershed in the Finger Lakes Region of Central New York located downwind from record setting Canadian forest fires during the summer of 2023. Daily sampling of stream and rainwaters was conducted over the 2 month smoke period, generating a robust geochemical dataset. Stream dissolved P showed high sensitivity to smoke events, attaining concentrations 2–3 × greater than the pre-smoke period. Subsequent rain events after smoke deposition were identified as a potentially important factor in magnitude and timing of dissolved P responses. These findings demonstrate the capacity for wildfire smoke to trigger rapid, observable changes to stream P chemistry.

Watershed biogeochemistry is rapidly being modified by enhanced wildfire activity in response to a changing climate. A less explored feature of wildfires are the smoke plumes released into the atmosphere and their impact on exposed watersheds situated downwind¹. Biomass burning injects around 34 – 41 million metric tons of aerosol smoke to the atmosphere per year². The smoke generated is rich in nutrients (such as C, P, K, Ca, Mg and to a lesser extent N) reflecting a portion of the pre-fire vegetation composition in the pyrolyzed biomass^{3–6}. Smoke plumes can be transported across large distances, impacting air quality in areas as far as 1000 km from active fires⁷. With an uncertain future in fire productivity^{8–10} as the Earth system continues to be modified through human-driven activities, the potential magnitude of smoke effects on the biogeochemical cycling of undisturbed watersheds remains a critical knowledge gap.

Most of our current understanding on smoke-driven biogeochemical impacts derives from research on nutrient-limited aquatic^{11–16} and tropical^{14,17–19} ecosystems heavily reliant upon nutrient delivery from external, atmospheric sources. In forested watersheds with temperate and Mediterranean climates, efforts to characterize atmospheric influences on the overall nutrient budget focus on dust deposition^{20–22}. These studies have demonstrated the importance of dust as an external supply of nutrients to such watersheds, outpacing bedrock weathering contributions in some instances²¹. While wildfire smoke has garnered considerably less attention in this respect, recent work suggests smoke could operate in a similar fashion²³ and potentially equal or surpass dust atmospheric nutrients fluxes to watersheds over shorter timescales.

In the watershed literature, the importance of wet-deposition events (i.e., rainstorms) on stimulating biogeochemical “hot moments” has been well documented²⁴ and remains an area of active research^{25–27}. For example, stream solute fluxes during rain events make up 40 – 80% of the total annual export out of watersheds^{28–31}. We anticipate that wildfire smoke dry deposition events could have a similar impact in generating such hot moments of nutrient supply, notably when coupled with rain events. The high nutrient abundance and surface area to volume ratio for smoke particles (typically particle sizes at 1 to submicron scale)³² favors fast leaching⁶, quickly supplying nutrients to stream solute export fluxes. However, a lack of knowledge on post-smoke deposition interactions throughout the bio-, hydro-, and litho-spheres within a watershed and the timescales at which they operate make it challenging to properly evaluate such event-driven impacts on stream chemistry.

This paper serves as a step forward into the relatively underexplored field of wildfire smoke biogeochemical cycling in watersheds. Motivation for this work and findings produced are a result of research performed serendipitously when an actively monitored watershed in the Finger Lakes Region of Central New York, USA was unexpectedly exposed to a series of extreme wildfire smoke events during summer (2023) from active fires in Canada’s extensive boreal forests. A broad chemical survey was conducted on collected stream and rainwaters to better identify potential aqueous species that could be impacted by wildfire smoke deposition. From this suite of analyses, dissolved phosphorus (P) demonstrated the highest sensitivity to smoke events. Here we provide

evidence of the potential for wildfire smoke to deliver a considerable supply of P to stream export fluxes over short (daily to weekly) time-scales. The extent to which smoke-driven dissolved P signals can manifest in stream waters depends on the degree of P-limitation in the watershed biome and timing of rain events following deposition.

Overview of watershed study area, Canadian wildfire-derived smoke, and monitoring efforts

The Northeastern United States in the 2023 summer season was marked by anomalously active Canadian wildfires where ~ 18 million hectares (over 42 million acres) of Canadian boreal forests were consumed⁹. Large plumes of smoke generated from these fires traveled southeastwards, exposing large areas of the Northeast U.S., including our study area in Central New York (Fig. 1a), to hazardous air quality conditions. New York State Air Quality for the closest monitoring station to the study area (East Syracuse, ~ 76 km away) reported maximum PM_{2.5} concentrations of 403.1 $\mu\text{g m}^{-3}$ air (June 6th, 2023, Fig. 1b), 142.3 $\mu\text{g m}^{-3}$ air (June 29th, 2023), and 59.8 $\mu\text{g m}^{-3}$ air (July 17th, 2023). Averaged hourly PM_{2.5} timeseries data collected from three local PurpleAir sensors (Fig. 1a) reported similar timing and relative magnitude of peaks in PM_{2.5} to those observed by New York State Air Quality (Table 1). The smoke period persisted for 2 months from beginning of June to end of July. Three smoke events were identified based on New York State Air Quality and local PurpleAir sensor PM_{2.5} observations (Fig. 1a) combined with estimated smoke parcel trajectories using the well-established HYSPLIT³³ model and satellite imaging approaches. These model results show most smoke was sourced from intense wildfires in Québec (5 million hectares burned, Fig. 1c, Table 1), located ~ 700 km upwind of the study area. The first two smoke events exceeded a threshold 101 $\mu\text{g m}^{-3}$ air considered “unhealthy” according to EPA’s Air Quality Index (AQI). The average duration of smoke events was ~ 5 days. The first event in early June

was among the shortest, but most intense (4.2 days, mean daily PM_{2.5} = 70.0 $\mu\text{g m}^{-3}$ air).

The study site, Cascadia Creek Gorge, is a temperate semi-urban watershed ideally situated to evaluate potential smoke perturbations to stream chemistry. Active stream environmental monitoring at daily to weekly sampling frequencies, initiated a year and a half prior to the smoke period (April 2022), provided a robust pre-smoke record that can be leveraged to evaluate smoke impacts; and, further, made us uniquely prepared to deploy a rapid sampling campaign in response to smoke events. Features such as a small basin area (36.67 km²) and gorge-based geomorphology yield strongly responsive (i.e., fast flushing) hydrologic behavior, conductive to tracking (hydro)biogeochemical dynamics at the event scale. Cascadia Creek is one of several southern tributaries to Cayuga Lake, the second largest of the Finger Lakes part of the broader Lake Ontario Basin³⁴. The main stem is classified as a 2nd order stream and drains a dynamic, post-glacial landscape characterized by a gorge formed through active incision into Devonian aged shale-siltstone bedrock. The region has a mixed conifer forest biome and is characterized by mixed precipitation where snow constitutes 62% of the total mean annual precipitation (2540 mm)³⁵. Mean annual temperature is ~ 7.9 °C with warm summers (max T = 26.1 °C) and cold to frigid winters (min T = -10 °C)³⁵.

Stream and rainwater samples were collected on a daily and per rainfall event basis, respectively, during the 2 month smoke period (*Methods*). Phosphorus data generated is presented in a timeseries of stream dissolved P during the smoke period (Fig. 2a) compared against variables such as estimated stream discharge (Fig. 2b), and P.M._{2.5} concentrations and cumulative precipitation (Fig. 2c). Long-term monitoring timeseries of dissolved P along with temperature, turbidity, and dissolved nutrients (NO₃⁻, SO₄²⁻, K⁺, and Ca²⁺) are provided in the Supplementary Fig. 1. Two types of dissolved P are presented in this study, obtained

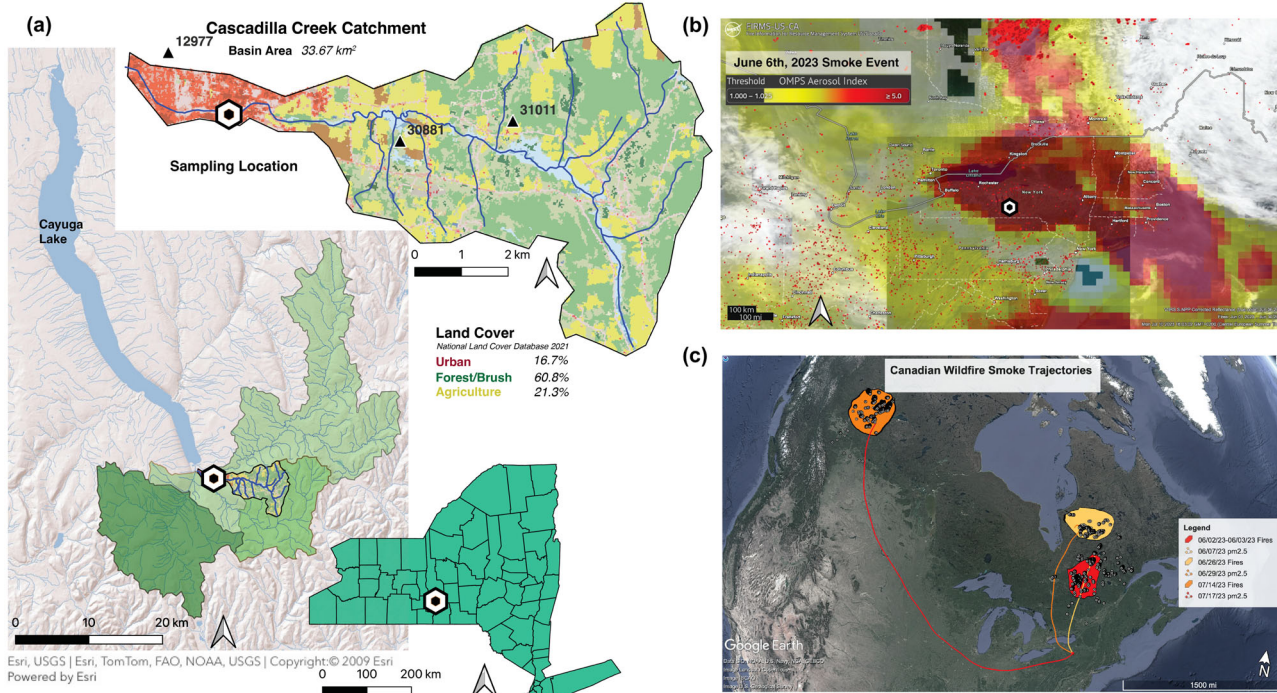


Fig. 1 | Description of the study area. **a** The location of Cascadia Creek watershed in the Finger Lakes Region of Central New York is provided along with the stream grab sampling location (honeycomb marker), PurpleAir sensors (filled triangles with station IDs), and land cover⁷³. Three PurpleAir sensors were selected given their relatively proximity (<10 km) to the sampling site located ~2 km (station 12977, Ithaca High School), ~4 km (station 30881, undefined forested area), and ~6 km (station 31011, Ellis Hollow Nature Reserve). Shaded green areas represent adjacent sub-watersheds to the study area from right to left Fall Creek (lightest

shading), Six Mile Creek and Cayuga Inlet (darkest shading) – all representing the major southern tributaries to the Cayuga Lake watershed. **b** Peak of Canadian wildfire smoke in June using MODIS and FIRMS satellite image data^{74,75} where coloring corresponds to the unitless OMPS (Ozone Mapping and Profiler Suite) Aerosol Index ranging from 0 (white) to ≥ 5 (red)⁷⁶. A value ≥ 5 indicates high aerosol concentrations capable of impacting human health and greatly reducing visibility. **c** Results from HYSPLIT air parcel backtracking using PM_{2.5} measurements (see *Methods*).

Table 1 | Smoke events and responses of peak stream dissolved P concentrations

Smoke periods				Peak stream dissolved P			Lag response to smoke
Start-end	Smoke origin	duration	Peak	Peak	Date time	Value ^c	Days
June 5th to June 9th	Québec, Canada	4.21	06/07 10:00	298.76	06/12 21:22	57.53 (19.14)	5.47
June 27th to July 3rd	Québec, Canada	6.63	06/29 08:00	122.36	06/27 15:57	92.68 (46.44)	20.25
					07/03 17:02	142.97 (105.54)	26.29 (4.38) ^d
July 16th to July 20th	British Columbia, Canada	3.54	07/04 17:00	55.62	07/17 17:08	80.85 (30.63)	40.30 (13)

^a Datetime is depicted here as MM/DD HH:HH where time corresponds to the local Eastern Standard Time (EST) time zone.

^b Peak PM_{2.5} values in units of $\mu\text{g m}^{-3}$ _{air}

^c Stream dissolved P concentrations presented in units of ppb ($\mu\text{g L}^{-1}$) and are shown in the following format: TDP (SRP). Total dissolved P (TDP) concentrations are shown first followed by Soluble Reactive P (SRP), which is italicized in parentheses.

^d Cumulative days from peak PM_{2.5} in the first smoke event are shown first, followed by response of peak dissolved P to most recent smoke event.

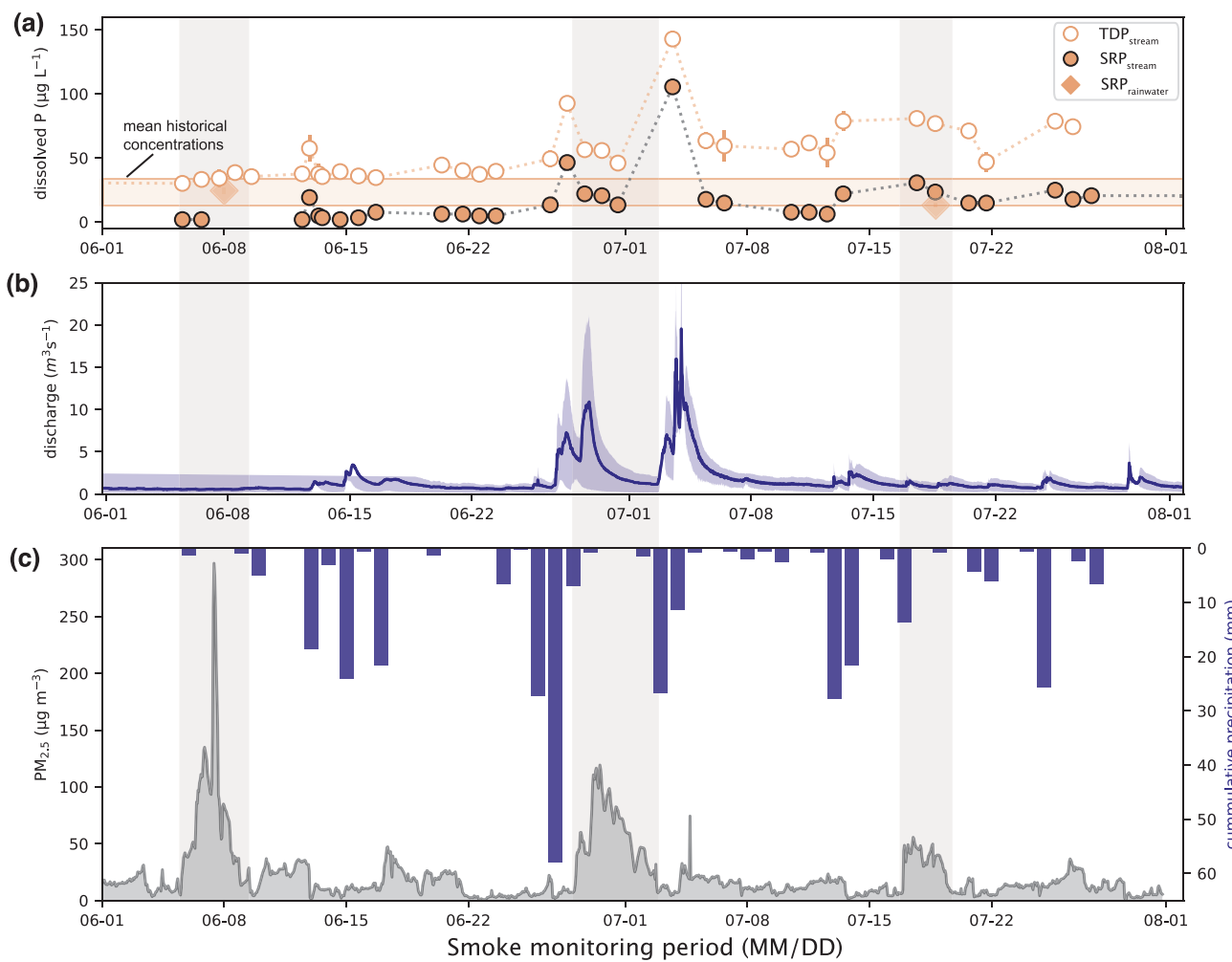


Fig. 2 | Stream dissolved P timeseries over the smoke period. Total dissolved (TDP) and soluble reactive (SRP) phosphorus data collected from stream and rainwaters during the 2 month smoke period are provided in a timeseries (a) alongside estimated stream flow (Methods) for Cascadilla Creek (b) and cumulative rainfall (NRCC) and PM_{2.5} measurements (c) from PurpleAir sensors nearby sampling location (Fig. 1). Gray shading indicates major smoke events identified

through HYSPLIT particle back tracking model results (Methods, Fig. 1c) and New York State Air Quality observations. Blue shading accompanying the estimated stream flow (b) represents standard deviation reported as 1σ . Mean historical streamwater concentrations combine this study's 1.5 year "pre-smoke" data and a 20 year record of dissolved P for the Cayuga Lake Watershed acquired from the Community Science Institute surface water database (a).

through distinct analytical protocols (Methods): Soluble Reactive P (SRP, defined as $\text{PO}_4\text{-P}$ or orthophosphate as P) and total dissolved P (TDP). Total dissolved P was continuously monitored as part of a global geochemical survey that was the initial focus of long-term monitoring efforts. Soluble Reactive P was only measured during the smoke period in response to the impromptu and unprecedented smoke event.

Results and discussion

Stream dissolved P dynamics during the smoke period

Stream dissolved P concentrations were found to be significantly elevated throughout the smoke period compared to historical watershed and regional observations. During the smoke period, SRP was on average higher (50.52 ± 59.39 ppb, $n = 31$) compared to a 20 year record for stormwaters of

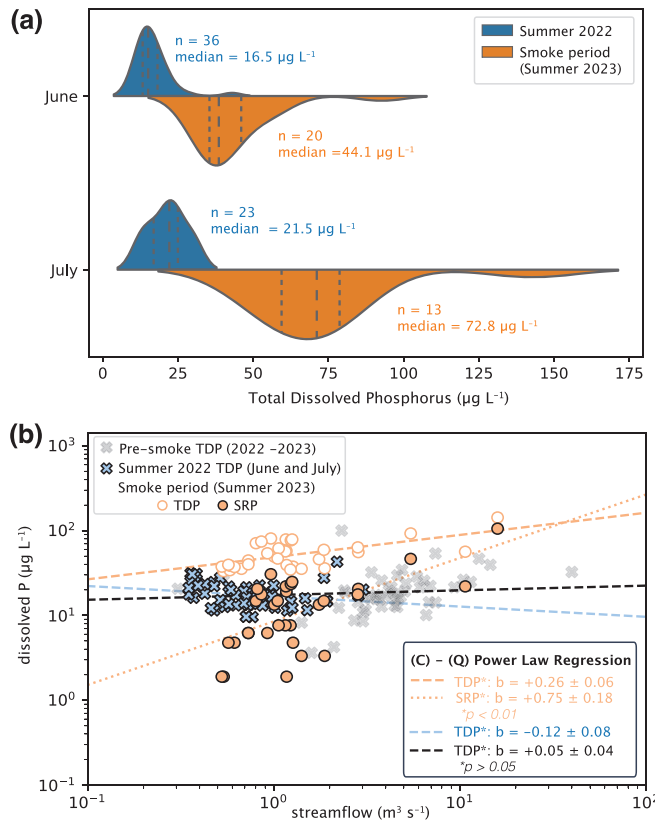


Fig. 3 | Comparing smoke-period stream dissolved P to historical observations. a Stream TDP data for the smoke influenced months of June and July are compared against “pre-smoke” data for identical months during the previous summer (2022) using a split violin plot. Dashed lines correspond to the median (middle) and 25% (left) and 75% (right) percentiles. b Phosphorous concentration vs. discharge plot is also shown for smoke SRP (filled orange circles) and TDP (open orange circles) compared against total “pre-smoke” (gray markers and black dashed line) and Summer 2022 June and July (for direct comparison with smoke period, blue markers and dashed line) TDP observations. Power law regression analyses are also provided and serve to distinguish between solute chemostatic (b value = 0 ± 0.2), dilution (b value < -0.2), and mobilization (b -value $> +0.2$) behavior with changing streamflow^{48–50}. Statistical significance of power law relationships was evaluated through Ordinary Least Squares (OLS) regression analyses.

all tributaries within the Cayuga Lake Watershed ($26.77 \pm 56.07 \text{ ppb}$, $n = 1448$)³⁶. Similarly, average stream TDP ($55.38 \pm 22.93 \text{ ppb}$, $n = 33$) were $2.78 \times$ higher than those we observed at Cascadilla Creek over a 1.5 year sampling period ($19.91 \pm 11.41 \text{ ppb}$, $n = 107$). Maximum TDP and SRP reached values of $143 \pm 6 \text{ ppb}$ and $105 \pm 3 \text{ ppb}$ simultaneously in early July. For this sample, SRP constituted $\sim 74\%$ of the TDP, which was the highest SRP fraction observed compared to the smoke duration average ($\sim 24\%$ of TDP). Discrepancy between smoke and pre-smoke periods is further accentuated when stream TDP is compared against data obtained for an equivalent time the previous summer (June and July 2022, Fig. 3a).

To determine potential drivers of stream dissolved P temporal variability during the smoke period, correlation analyses were conducted on a suite of relevant environmental variables evaluated between the 2023 “smoke” and 2022 “non-smoke” summer periods (Fig. 4). Stream dissolved P was weakly correlated with $\text{PM}_{2.5}$ (Fig. 4a), $r = -0.14$, $p = 0.429$ (TDP) and $r = -0.10$, $p = 0.588$ (SRP). Relative peaks in TDP and SRP appear lagged with respect to peaks in $\text{PM}_{2.5}$ (Fig. 2, Table 1). The extent of these lagged responses (cumulative response to first smoke event range of $\sim 5.5 - \sim 40$ days) appears to depend on the timing of rain following a smoke event. Stream TDP and SRP are highly, positively correlated to discharge (TDP: $r = +0.67$, $p < 0.001$; SRP: $r = +0.82$, $p < 0.001$) and moderately correlated to turbidity (TDP: $r = +0.45$, $p < 0.05$; SRP: $r = +0.58$,

$p < 0.001$) during the smoke period compared to its “non-smoke” counterpart (Fig. 4b). These results complement concentration (C)–discharge (Q) power law relationships ($C = aQ^b$), a common metric for solute mobility behavior in catchments^{37–39} applied to stream TDP and SRP (Fig. 3b). Results indicate moderate ($b = +0.26 \pm 0.06$, $R^2 = 0.34$) and high ($b = +0.75 \pm 0.18$, $R^2 = 0.38$) flushing (or mobilization) behavior, respectively for TDP and SRP, during the smoke period compared to chemostatic behavior in TDP observed for non-smoke, summer 2022 ($b = -0.12 \pm 0.08$, $R^2 = 0.04$, $n = 59$) and overall pre-smoke long-term monitoring (April 2022–May 2023; $b = +0.05 \pm 0.04$, $R^2 = 0.11$, $n = 109$). Contrasting dissolved P export behavior between summertime pre-smoke and smoke mitigates the plausibility of seasonal variability as an alternative explanation for observed C–Q relations. Event-scale flushing behavior in stream dissolved P is consistent with prior studies focused on watersheds with heavy agricultural or urban land use^{40–44} where enriched shallow, soilwater P pools (generally anthropogenically-derived) drive observed increases in dissolved P concentrations with increasing discharge. We are currently unaware of any study demonstrating smoke influenced dissolved P mobilization at event timescales.

Smoke-derived P as a driver of observed stream concentrations

High stream dissolved P during the smoke period, while notable, is not alone sufficient to demonstrate smoke driven effects. Urban and agricultural areas, important reservoirs of P in the region from storm drainage and fertilizer application^{34,36,45,46}, together constitute 38% of Cascadilla Creek’s land cover³⁴ (Fig. 1a). Sensitivity of stream dissolved P export fluxes in response to rain events is widely observed and generally associated with the flushing of anthropogenic P^{45–49}. This excess P supply to surface waters greatly impacts water quality and contributes to occurrences of harmful algal blooms in Cayuga Lake and Great Lakes Basin more broadly⁵⁰. Maximum “pre-smoke” stream TDP concentrations for Cascadilla Creek occurred during the winter months ($100.22 \pm 10.02 \text{ ppb}$, February 2023) when manure is generally applied on agricultural lands³⁴. Even during a particularly dry summer in 2022 where monthly precipitation was 42 mm (June) and 89 mm (July), $\sim 2.6 \times$ less than observed in 2023³⁵, maximum stream TDP attained during storm events never exceeded 50 ppb. Thus, while the partial influence of anthropogenic sources to our stream data cannot fully be discounted, historical observations suggest this is minimal. We can further support this assessment through two key lines of evidence that favor smoke-driven contributions to stream dissolved P.

We first readily demonstrate that wildfire smoke can supply large quantities of P to our study area. Canadian coniferous forests are known to hold large stocks of P in their foliage and litter biomass pools^{51,52}. For such forest types, a representative C:P stoichiometry ratio is $\sim 1000 \mu\text{g P g C}^{-1}$ ⁵². We can treat this as a maximum value for the aerosol C:P ratio given the low volatility of P compared to C⁵³. Biomass burning is estimated to release $\sim 60\%$ of biomass P to smoke aerosols^{3–5,18}. Using a C:P ratio of $1000 \mu\text{g P g C}^{-1}$ we can approximate smoke P deposition rates (*Methods*), which range from $2 - 116 \mu\text{g m}^{-2} \text{ day}^{-1}$ (mean = $20 \mu\text{g m}^{-2} \text{ day}^{-1}$). Accounting for the watershed area ($\sim 37 \text{ km}^2$), roughly 40 kg of P was deposited over the 2 month period; $\sim 70\%$ of which were deposited in the first two smoke events (Fig. 2). Leaching rates from laboratory experiments^{54,55} suggest smoke-soilwater interaction times between 7 – 22 h are needed to obtain peaks in stream dissolved P—more than sufficient time for post-deposition smoke dissolution and flushing via ensuing rain. Detectable levels of TDP and SRP in rainwaters (Fig. 2a) collected from light drizzle conditions during the most intense smoke period in early June (SRP = $29 \pm 2 \text{ ppb}$) and middle July (SRP = $13 \pm 2 \text{ ppb}$) further corroborate the presence of soluble P in deposited smoke particles. These aerosols most likely served as nucleation sites for water condensation under these weather conditions, facilitating partial leaching during deposition⁵⁶.

Stream TDP can also be compared against a known smoke tracer, K^+ (Fig. 5a), another bioavailable nutrient found readily in $\text{PM}_{2.5}$ ^{7,23,32}. A statistically significant positive trend emerges during the smoke period ($R^2 = 0.72$, $p < 0.01$) that falls outside the confidence interval for pre-smoke

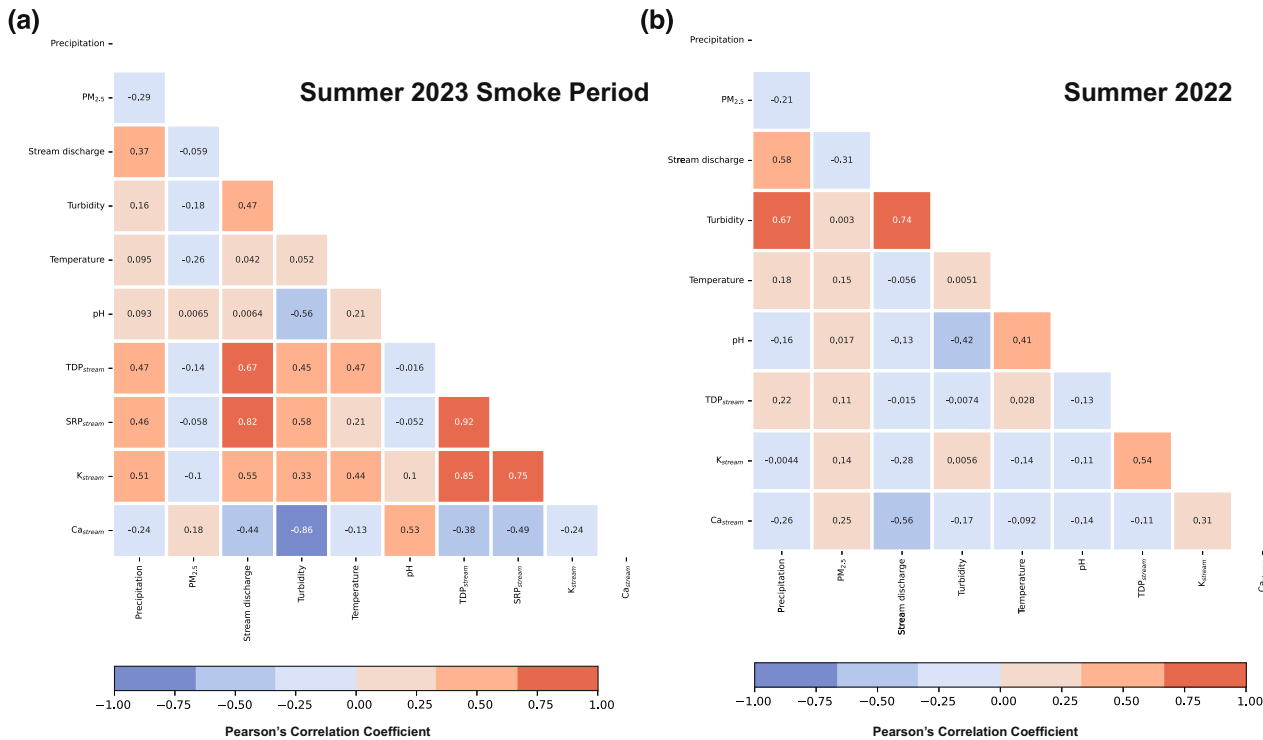


Fig. 4 | Pearson correlation matrix for 2023 smoke period versus the previous “pre-smoke” summer. Color gradient represents strength and directionality of the Pearson correlation coefficient across a set of smoke, precipitation, and stream physiochemical and dissolved concentration variables of interest. A strong negative or positive correlation is indicated by -1 (dark blue) and $+1$ (dark red), respectively,

whereas a coefficient of 0 signifies no correlation (light blue/red). Summertime smoke period in 2023 (a) correlations are compared with equivalent time periods to the smoke monitoring period (June and July) from the prior, pre-smoke summer 2022 (b). Pearson correlation coefficients were determined using the Python open-sourced science computing library, SciPy⁷⁷.

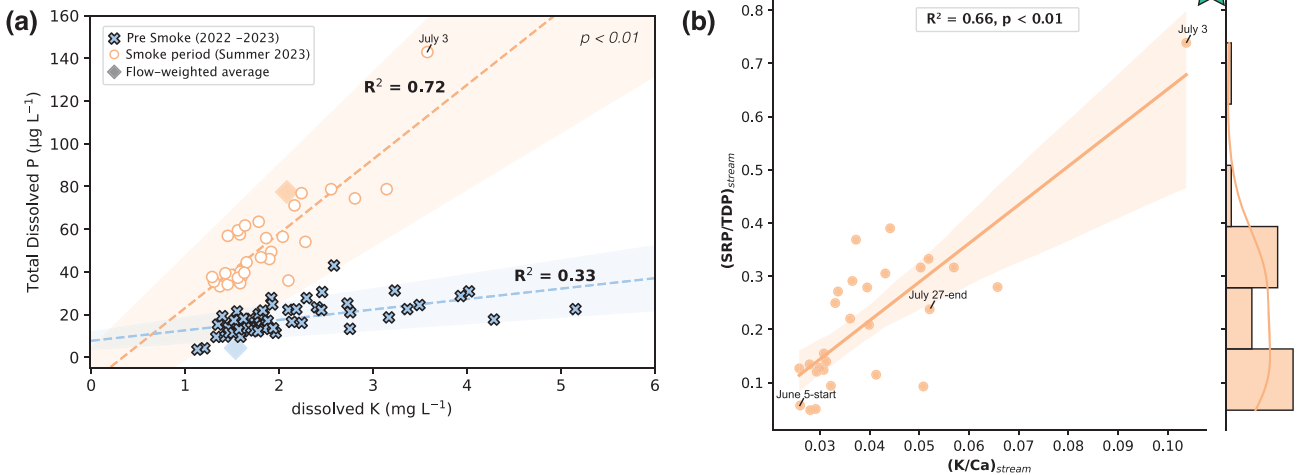


Fig. 5 | Stream dissolved P evaluated against a smoke tracer. **a** Stream TDP is shown against dissolved K^+ , a traditional in-direct tracer of smoke contributions for both the “pre-smoke” and smoke period. Flow-weighted average for both datasets is included for context. **b** Smoke period stream SRP/TDP versus dissolved K^+ normalized to Ca^{2+} . Star symbol reflects composition of rainwater collected during dry deposition and represents a smoke leaching endmember. Histogram distributions

are provided alongside the linear trend to show overall data structure. The smoke period exhibited positive trends for both plots **a** ($R^2 = 0.72$) and **b** ($R^2 = 0.66$). Ordinary Least Squares regression was utilized for both plots to evaluate the linear trends and their statistical significance (p -value) based on two-tailed tests. Shaded areas correspond to the linear regression 95% confidence interval.

historical data ($R^2 = 0.33$, $p < 0.01$). Since dissolved K^+ is also sourced by bedrock weathering, we can normalize it to another known weathering-derived element, Ca^{2+} (as was done by Evans et al., 2021²³), to correct for this influence. Evans et al. ²³ found elevated K in stream dissolved concentrations

compared to Ca during smoke years, indicative of smoke contributions of K to the watershed. Stream dissolved P can also be presented as the ratio of SRP/TDP since dissolved P released by smoke leaching is predominantly in bio-available or soluble P form⁵⁷. When stream SRP/TDP are evaluated

against K/Ca ratios (Fig. 5b) during the smoke period, we find the positive trend still holds ($R^2 = 0.66, p < 0.01$). It is, however, important to stipulate that this trend is contingent on the July 3rd, 2023 datapoint, defining the uppermost bound of the overall data structure (Fig. 5b), and loses statistical significance when removed ($R^2 = 0.35, p > 0.5$). Rain “drizzle” water from the first smoke event plot on the upper portion of this plot with SRP/TDP ~ 1 (i.e., $\sim 100\%$ SRP) and a K/Ca mass ratio of 0.36 and serve as a representative smoke leaching endmember. The linear trend observed in stream waters towards this endmember in Fig. 5b provides further evidence in support of smoke-derived P to observed stream dissolved P behavior during the smoke period.

Smoke signals in streams and wider implications for watershed P biogeochemical cycling

Our findings reveal strong event-driven smoke signals in stream dissolved P concentrations within an undisturbed, temperate watershed. Smoke event intensity and timing of ensuing rain events are likely drivers dictating the sensitivity and magnitude of stream dissolved P responses. This implies that forested watersheds in wetter climates may be more sensitive to event-driven smoke impacts to stream chemistry. Conversely in drier climates where rain events after appreciable smoke deposition are less frequent (smoke seasons generally taking place during the driest part of the year)⁷ or in watersheds dominated by seasonal, spring snowmelt (such as montane catchments) 9+ months after smoke deposition during the previous summer, smoke signals in streams could be overprinted by a variety of seasonal processes controlling nutrient export dynamics. Given the serendipitous nature of this work, limitations in our dataset (stream and rainwater focused, single watershed) prevent adequate exploration of these hypotheses. Future work is needed to explore the extent of event-driven smoke nutrient supply to watersheds across climate and geomorphic gradients, leveraging more robust smoke tracers such as black carbon^{14,32,58} and synoptic sampling of both dry and wet deposition. Further, in-situ leaching of smoke aerosols within soil porewaters is hypothesized to be the main process driving smoke-sourced P export; but an important caveat is the positive correlation with turbidity (TDP: $r = +0.45, p < 0.05$), which suggests smoke adsorption on soils as another plausible export pathway. Future work is required to fully evaluate smoke-derived nutrient export mechanisms from watersheds.

A comparable study to this one explicitly investigated wildfire smoke impacts on the stream solute chemistry of an undisturbed watershed in British Columbia found strong sensitivity of N and K to smoke, with negligible changes to dissolved P²³. These findings are opposite to our observations, extending to dissolved N which we found to be minimally impacted by smoke. One potential explanation could be the low, annual sampling frequency that may “miss” important synoptic-scale behavior. Variability in smoke particle geochemical stoichiometry^{59–61} arising from heterogeneity in source biomass burned⁵² and volatilization behavior of C and N is also a potentially important factor. Another alternative, postulated by Evans et al. (2021)²³, is the mobility of N and P in the watershed ecosystems—i.e., the forest nutrient economy and extent of nutrient limitation^{62–64}. Strong P retention may occur in P-limited forest ecosystems, suppressing smoke signals in dissolved P export fluxes by tightly cycling smoke P contributions within the system. Following this logic, conflicting results between our studies may be a consequence of differing nutrient limitations between P-limited²³ and N-limited⁶⁵ (this study) ecosystems. Further, excess supply of P and N through atmospheric deposition has been shown to shift ecosystem N, P limitation^{66,67} demonstrating that nutrient limitation is dynamic and can shift in response to changing atmospheric nutrient supply. In this respect, wildfire smoke prevalence in the future could have long-term consequences¹⁵; potentially augmenting widespread increases in stream dissolved P already observable at the Great Lakes Basin scale and, notably, associated with more frequent occurrences of HABs⁵⁰.

Methods

Sample collection

Streamwaters. Stream samples were collected by hand into acid-cleaned 250 mL Nalgene bottle and a 4 mL scintillation vial. In the field, the 250 mL bottle was rinsed 3x with Cascadia Creek water prior to collection of the Cascadia Creek water. At time of collection, general stream chemistry measurements were recorded in-situ using a YSI ProDSS Multiparameter Digital Water Quality Meter which had 4 probes attached to it (pH, turbidity, chloride, specific conductivity). The probes were left in Cascadia Creek for a minimum of 5 min to allow stabilization before recording measurements. A HOBO Water Level and a HOBO Fresh Water Conductivity Data Loggers were deployed ~ 50 m upstream from sample collection and took measurements at 2.5 min intervals to record specific conductivity and stream depth over time. Stream grab samples were filtered in the lab (~ 100 m from sampling location) with a 0.2 μm filter. Samples were split into 3 separate aliquots, ~ 100 mL for anion analysis, ~ 100 mL for cation and P analysis, and ~ 25 mL for alkalinity analysis. The remaining sample was used for laboratory-based pH measurement.

Rainwater. An Aerochem National Trends Network deposition collector was used to collect precipitation samples. The deposition collector has 2 buckets that collect either dry deposition or wet deposition depending on the presence of moisture on a 7-grid sensor. Rain samples followed similar post-collection protocols to the streamwaters outlined above.

Chemical analyses

Cations and elemental analyses. Samples collected for cation analysis were acidified using HNO₃ and then analyzed on a Spectroblue ICP-OES. Samples were run for Al, Ca, Fe, K, Mg, Mn, Na, S, Si, Sr, P, and Zn. An important distinction for ICP methodology when compared to the use of an HPLC and/or a UV-VIS is that total concentrations regardless of form are recorded. As such, since samples were filtered before being run on the ICP-OES, measurements provided of P concentrations are of Total Dissolved Phosphorous (from here on TDP). The limit of detection for the ICP-OES was 8.38 ppb with a standard error of 1.41 ppb.

UVVis spectrophotometry. The molybdate blue colorimetric method⁶⁸ was the standard protocol used for the determination of soluble reactive phosphorus (SRP), presented in the study as PO₄³⁻, used. This procedure involves reducing 30 mL sample with ascorbic acid and addition of a mixed reagent containing ammonium molybdate, potassium antimony tartrate, and sulfuric acid. Measurements were taken at an absorbance wavelength of 880 nm with 10 cm path length quartz cuvettes. Limit of detection for this protocol was 5 ppb with a long-term precision of $\pm 10\%$ for low (< 10 ppb) and $\pm 5\%$ for intermediate-high (50 ppb–1 ppm) SRP abundance.

Anions. Anion samples collected from Cascadia Creek were analyzed by an HPLC (Shimadzu Nexera High Pressure Liquid Chromatography). Samples were pipetted into 2 mL vials and then transferred to the auto-sampler rack before being run. Measured anions include F⁻, Cl⁻, NO₃⁻, and CHO₂⁻, PO₄³⁻, and SO₄²⁻. Standard concentrations ranged from 50 ppb to 20 ppm ($n = 8$) and included a blank at the start of each run. The analytical column (Shodex SI-52 4E) was set to 40 °C. Samples were run for 31 min to allow all peaks to be resolved before the introduction of a new sample. The limit of detection was determined to be 50 ppb, serving as a higher end member of detection for stream waters and precipitation.

Air parcel trajectories

Smoke parcels were tracked using HYSPLIT³³, NASA’s Modern-Era Retrospective Analysis for Research and Applications⁶⁹, PurpleAir in-situ sensors, and Fire Information for Resource Management System (FIRMS). Backwards trajectories at 3000 m were run for 24–72 h using Snee Hall, Cornell University, Ithaca, NY (Lat = 42.2234, Long = -76.4846), ~ 400 m

from stream sampling location. Trajectories were ran using the hour of peak PM_{2.5} concentrations in Ithaca, NY. 3 smoke events were used, one on June 7, 2023, another on June 29, 2023, and the third event being July 17, 2023. Trajectories were then imported into Google Earth Pro, where the end of the trajectories (i.e., the “source” of the smoke event) were then used as the source area and timing of analysis.

Surface PM_{2.5} concentrations were acquired from in-situ PurpleAir⁷⁰ sensor located nearby the study area (Fig. 1). Dates from the end of the HYSPLIT trajectories (1–3 days before peak PM_{2.5} concentrations) were used to see if the HYSPLIT-predicted sourcing of smoke matched the reanalysis of surface PM_{2.5} concentrations. In addition to HYSPLIT, FIRMS was utilized to identify fire hot spots on predicted dates of smoke sourcing. Archived data shapefiles were downloaded from FIRMS to visualize fires along with HYSPLIT trajectories in Google Earth Pro.

Stream discharge

Due to a lack of functional gauges throughout Cascadilla watershed, stream discharge was measured during grab sampling using a flow probe meter and measurements of stream depth and width. To accommodate the low-resolution data this technique affords, 15 min interval stream discharge data from adjacent USGS gauged watersheds Fall Creek (basin area = 326 km²) and Six Mile Creek (basin area = 101 km²) were used to estimate discharge at Cascadilla Creek. We leveraged a traditional approach⁴⁶ that estimates flow rates at our poorly gauged site (Q_{Casc}) from the product of flow data from the adjacent watershed (Q_i where i = Fall or Six Mile Cr.) and ratio of the watershed areas (A) as follows:

$$Q_{Casc} = Q_i * \frac{A_i}{A_{Casc}} \quad (1)$$

Six Mile Creek was used as a test dataset (2020–2023) using Fall Creek flow data to evaluate the effectiveness of the approach to predict stream discharge. Observed and predicted flow values for the Six Mile Cr. test dataset yielded a Nash-Sutcliffe Efficiency (NSE, a commonly used metric for goodness of fit)⁷¹ score of 0.68, which indicates a good predictive performance for this approach. The Six Mile Cr. flow data was then used to predict Cascadilla Creek discharge over the environmental monitoring period (Apr. 2022 to Aug. 2023). Predictions were able to adequately replicate our sparse streamflow data collected from grab measurements (NSE = 0.77).

Smoke P deposition rate estimations

An estimate of P deposition rates can be calculated using a traditional formula for dry depositional fluxes (F_d , units of $\mu\text{g m}^{-2} \text{ day}^{-1}$) of atmospheric aerosols¹²:

$$F_d = V_d * C_d \quad (2)$$

where V_d corresponds to the depositional velocity (m s⁻¹) and C_d is the concentration ($\mu\text{g m}^{-3}$). A depositional velocity of 1.0 cm s⁻¹ was chosen as a reasonable approximation for smoke aerosol particle sizes between 0.1 to 1 μm based on observations for deposition on coniferous forests⁷². The smoke P dry depositional concentration was estimated by taking the hourly PM_{2.5} dataset and converting it to $\mu\text{g P m}^{-3}$ using a maximum smoke C:P stoichiometry of 1000 $\mu\text{g P g C}^{-1}$ representative of pre-burned coniferous forests⁵². This calculation assumes smoke aerosols are comprised principally of pyrogenic carbon³⁸.

Reporting summary

Further information on research design is available in the Nature Portfolio Reporting Summary linked to this article.

Data availability

Stream and rainwater geochemical data presented in this study (Table 1, Figs. 2–5) are hosted in the open source repository CUAHSI HydroShare and can be accessed at Fernandez, N., H. Jamison, Z. Gold (2024). Stream and

rainwater geochemical (dissolved P, K, and Ca), stream discharge, meteorologic and aerosol concentration datasets for Cascadilla Creek (Central New York, USA), HydroShare, <https://doi.org/10.4211/hs.a339c49566c04c9092f04d5895a1ef09> (shared under the Creative Commons Attribution CC BY). Compiled cumulative daily precipitation, PM_{2.5}, and estimated streamflow values are additionally provided in HydroShare repository (Table S2 and S3). Stream discharge datasets used for estimating Cascadilla Creek streamflow Figs. 2b and 3b and Supplementary Fig. 1 derives from <https://waterdata.usgs.gov/usa/nwis>. Meteorologic (cumulative daily precipitation) and PM_{2.5} aerosol concentration data used in Figs. 2c and 4 as well as Table 1 (for PM_{2.5}) derive from the Northeast Regional Climate Center (NRCC) CLIMOD-2 (<http://climod2.nrcc.cornell.edu/>) and PurpleAir API, respectively.

Received: 28 November 2023; Accepted: 25 September 2024;

Published online: 04 October 2024

References

1. David, A. T., Asarian, J. E. & Lake, F. K. Wildfire smoke cools summer river and stream water temperatures. *Water Resour. Res.* **54**, 7273–7290 (2018).
2. Schill, G. P. et al. Widespread biomass burning smoke throughout the remote troposphere. *Nat. Geosci.* **13**, 422–427 (2020).
3. Kauffman, J. B., Cummings, D. L. & Ward, D. E. Relationships of fire, biomass and nutrient dynamics along a vegetation gradient in the Brazilian Cerrado. *J. Ecol.* **82**, 519–531 (1994).
4. Kauffman, J. B., Cummings, D. L., Ward, D. E. & Babbitt, R. Fire in the Brazilian Amazon: 1. biomass, nutrient pools, and losses in slashed primary forests. *Oecologia* **104**, 397–408 (1995).
5. Pivello, V. R. & Coutinho, L. M. Transfer of macro-nutrients to the atmosphere during experimental burnings in an open cerrado (Brazilian savanna). *J. Tropical Ecol.* **8**, 487–497 (1992).
6. Baker, A. R., Jickells, T. D., Witt, M. & Linge, K. L. Trends in the solubility of iron, aluminium, manganese and phosphorus in aerosol collected over the Atlantic Ocean. *Mar. Chem.* **98**, 43–58 (2006).
7. Valerino, M. J. et al. Sources and composition of PM_{2.5} in the Colorado front range during the DISCOVER-AQ study. *J. Geophys. Res. Atmos.* **122**, 566–582 (2017).
8. Jolly, W. M. et al. Climate-induced variations in global wildfire danger from 1979 to 2013. *Nat. Commun.* **6**, 7537 (2015).
9. Barnes, C. et al. *Climate Change More than Doubled the Likelihood of Extreme Fire Weather Conditions in Eastern Canada*. <https://www.worldweatherattribution.org> (2023).
10. Andela, N. et al. A human-driven decline in global burned area. *Science* **356**, 1356–1362 (2017).
11. Vicars, W. C., Sickman, J. O. & Ziemann, P. J. Atmospheric phosphorus deposition at a montane site: Size distribution, effects of wildfire, and ecological implications. *Atmos. Environ.* **44**, 2813–2821 (2010).
12. Markaki, Z. et al. Atmospheric deposition of inorganic phosphorus in the Levantine Basin, eastern Mediterranean: Spatial and temporal variability and its role in seawater productivity. *Limnol. Oceanogr.* **48**, 1557–1568 (2003).
13. Hamilton, D. S. et al. Recent (1980 to 2015) trends and variability in daily-to-interannual soluble iron deposition from dust, fire, and anthropogenic sources. *Geophys. Res. Lett.* **47**, e2020GL089688 (2020).
14. Barkley, A. E. et al. African biomass burning is a substantial source of phosphorus deposition to the Amazon, Tropical Atlantic Ocean, and Southern ocean. *Proc. Natl. Acad. Sci. USA* **116**, 16216–16221 (2019).
15. Scordo, F. et al. Smoke from regional wildfires alters lake ecology. *Sci. Rep.* **11**, 10922 (2021).
16. Goldman, C. R., Jassby, A. D. & de Amezaga, E. Forest fires, atmospheric deposition and primary productivity at Lake Tahoe, California-Nevada. *SIL Proceedings* **24**, 499–503 (1990).

17. Gao, Y. et al. Effects of atmospheric reactive phosphorus deposition on phosphorus transport in a subtropical watershed: A Chinese case study. *Environ. Pollution* **226**, 69–78 (2017).
18. Mahowald, N. M. et al. Impacts of biomass burning emissions and land use change on Amazonian atmospheric phosphorus cycling and deposition. *Global Biogeochem. Cy.* <https://doi.org/10.1029/2005GB002541> (2005).
19. Mahowald, N. et al. Global distribution of atmospheric phosphorus sources, concentrations and deposition rates, and anthropogenic impacts. *Global Biogeochem. Cy.* <https://doi.org/10.1029/2008GB003240> (2008).
20. Arvin, L. J., Riebe, C. S., Aciego, S. M. & Blakowski, M. A. Global patterns of dust and bedrock nutrient supply to montane ecosystems. *Sci. Adv.* **3**, 1–11 (2017).
21. Aciego, S. M. et al. Dust outpaces bedrock in nutrient supply to montane forest ecosystems. *Nat. Commun.* **8**, 14800 (2017).
22. Aarons, S. M. et al. Geochemical characterization of critical dust source regions in the American West. *Geochimica et Cosmochimica Acta* **215**, 141–161 (2017).
23. Evans, J. S., Norman, A.-L. & Reid, M. L. Evidence of smoke from wildland fire in surface water of an unburned watershed. *Water Resour. Res.* **57**, e2021WR030069 (2021).
24. McClain, M. E. et al. Biogeochemical hot spots and hot moments at the interface of terrestrial and aquatic ecosystems. *Ecosystems* **6**, 301–312 (2003).
25. Dwivedi, D., Arora, B., Steefel, C. I., Dafflon, B. & Versteeg, R. Hot Spots and Hot Moments of Nitrogen in a Riparian Corridor. *Water Resour. Res.* **54**, 205–222 (2018).
26. Mehdi, B., Schürz, C., Grath, B. & Schulz, K. Storm event impacts on in-stream nitrate concentration and discharge dynamics: a comparison of high resolution in-situ measured data with model simulations. *Sci. Total Environ.* **755**, 143406 (2021).
27. Wang, J. et al. Sampling frequency, load estimation and the disproportionate effect of storms on solute mass flux in rivers. *Sci. Total Environ.* **906**, 167379 (2024).
28. Larsen, M. C. & Simon, A. A rainfall intensity-duration threshold for landslides in a humid-tropical environment, Puerto Rico. *Geografiska Annaler Series A. Phys. Geogr.* **75**, 13–23 (1993).
29. Moatar, F. et al. Stream solutes and particulates export regimes: a new framework to optimize their monitoring. *Front. Ecol. Evol.* **7**, 1–19 (2020).
30. Raymond, P. A. & Sayers, J. E. Event controlled DOC export from forested watersheds. *Biogeochemistry* **100**, 197–209 (2010).
31. Yoon, B. & Raymond, P. A. Dissolved organic matter export from a forested watershed during Hurricane Irene. *Geophys. Res. Lett.* **39**, 1–6 (2012).
32. Sullivan, A. P. et al. A method for smoke marker measurements and its potential application for determining the contribution of biomass burning from wildfires and prescribed fires to ambient PM2.5 organic carbon. *J. Geophys. Res. Atmos.* <https://doi.org/10.1029/2008JD010216> (2008).
33. Stein, A. F. et al. NOAA's HYSPLIT atmospheric transport and dispersion modeling system. *Bull. Am. Meteorol. Soc.* **96**, 2059–2077 (2015).
34. Haith, D. A., Hollingshead, N., Bell, M. L., Kreszewski, S. W. & Morey, S. J. Nutrient loads to Cayuga Lake, New York: watershed modeling on a budget. *J. Water Resour. Plann. Manage.* **138**, 571–580 (2012).
35. NRCC. NRCC Home Page <https://www.nrcc.cornell.edu/> (2024).
36. O'Leary, N., Johnston, R., Gardner, E. L., Penningroth, S. M. & Bouldin, D. R. Long-term study of soluble reactive phosphorus concentration in fall creek and comparison to northeastern tributaries of Cayuga Lake, NY: Implications for watershed monitoring and management. *Water (Switzerland)* **11**, 2075 (2019).
37. Wymore, A. S. et al. Revisiting the origins of the power-law analysis for the assessment of concentration-discharge relationships. *Water Resour. Res.* **59**, e2023WR034910 (2023).
38. Evans, C. & Davies, T. D. Causes of concentration/discharge hysteresis and its potential as a tool for analysis of episode hydrochemistry. *Water Resour. Res.* **34**, 129–137 (1998).
39. Li, L. et al. Toward catchment hydro-biogeochemical theories. *Wiley Interdiscip. Rev. Water* **8**, 1–31 (2021).
40. Rose, L. A., Karwan, D. L. & Godsey, S. E. Concentration–discharge relationships describe solute and sediment mobilization, reaction, and transport at event and longer timescales. *Hydrological Processes* **32**, 2829–2844 (2018).
41. Siwek, J., Siwek, J. P. & Żelazny, M. Environmental and land use factors affecting phosphate hysteresis patterns of stream water during flood events (Carpathian Foothills, Poland). *Hydrol. Process.* **27**, 3674–3684 (2013).
42. Bieroza, M. Z. & Heathwaite, A. L. Seasonal variation in phosphorus concentration–discharge hysteresis inferred from high-frequency in situ monitoring. *J. Hydrol.* **524**, 333–347 (2015).
43. Haygarth, P. et al. Temporal variability in phosphorus transfers: classifying concentration–discharge event dynamics. *Hydrol. Earth Syst. Sci.* **8**, 88–97 (2004).
44. Thompson, S. E., Basu, N. B., Lascurain, J., Aubeneau, A. & Rao, P. S. C. Relative dominance of hydrologic versus biogeochemical factors on solute export across impact gradients. *Water Resour. Res.* **47**, 1–20 (2011).
45. Johnson, A. H., Bouldin, D. R., Goyette, E. A. & Hedges, A. M. Phosphorus loss by stream transport from a rural watershed: quantities, processes, and sources. *J. Environ. Qual.* **5**, 148–157 (1976).
46. Prestigiacomo, A. R. et al. Apportionment of bioavailable phosphorus loads entering Cayuga Lake, New York. *J. Am. Water Resour. Assoc.* **52**, 31–47 (2016).
47. McDowell, R. W. & Sharpley, A. N. Approximating phosphorus release from soils to surface runoff and subsurface drainage. *J. Environ. Qual.* **30**, 508–520 (2001).
48. Filippelli, G. M. The global phosphorus cycle: past, present, and future. *Elements* **4**, 89–95 (2008).
49. Andersen, H. E., Windolf, J. & Kronvang, B. Leaching of dissolved phosphorus from tile-drained agricultural areas. *Water Sci. Technol.* **73**, 2953–2958 (2016).
50. Singh, N. K., Van Meter, K. J. & Basu, N. B. Widespread increases in soluble phosphorus concentrations in streams across the transboundary Great Lakes Basin. *Nat. Geosci.* **16**, 893–900 (2023).
51. Vann, D. R. et al. Distribution and cycling of C, N, Ca, Mg, K and P in three pristine, old-growth forests in the Cordillera de Pichué, Chile. *Biogeochemistry* **60**, 25–47 (2002).
52. McGroddy, M. E., Daufresne, T. & Hedin, L. O. Scaling of C:N:P stoichiometry in forests worldwide: implications of terrestrial redfield-type ratios. *Ecology* **85**, 2390–2401 (2004).
53. Hungate, B. A. et al. *Disturbance and Element Interactions*. <https://ecos.nau.edu/publication/disturbance-element-interactions/> (2003).
54. Spencer, C. N. & Hauer, F. R. Phosphorus and nitrogen dynamics in streams during a wildfire. *J. N. Am. Benthol. Soc.* **10**, 24–30 (1991).
55. Boyer, E. W., Moritz, M. A. & Brown, M. G. Smoke deposition to water surfaces drives hydrochemical changes. *Hydrol. Process.* **36**, e14626 (2022).
56. Royer, H. M. et al. African smoke particles act as cloud condensation nuclei in the wintertime tropical North Atlantic boundary layer over Barbados. *Atmos. Chem. Phys.* **23**, 981–998 (2023).
57. Migon, C. & Sandroni, V. Phosphorus in rainwater: partitioning inputs and impact on the surface coastal ocean. *Limnol. Oceanogr.* **44**, 1160–1165 (1999).

58. Yu, P. et al. Black carbon lofts wildfire smoke high into the stratosphere to form a persistent plume. *Science* **365**, 587–590 (2019).

59. Turn, S. Q. et al. Elemental characterization of particulate matter emitted from biomass burning: Wind tunnel derived source profiles for herbaceous and wood fuels. *J. Geophys. Res. Atmos.* **102**, 3683–3699 (1997).

60. Reid, J. S. et al. Physical, chemical, and optical properties of regional hazes dominated by smoke in Brazil. *J. Geophys. Res. Atmos.* **103**, 32059–32080 (1998).

61. Echalar, F., Gaudichet, A., Cachier, H. & Artaxo, P. Aerosol emissions by tropical forest and savanna biomass burning: characteristic trace elements and fluxes. *Geophys. Res. Lett.* **22**, 3039–3042 (1995).

62. Grimm, N. B. et al. Merging aquatic and terrestrial perspectives of nutrient biogeochemistry. *Oecologia* **137**, 485–501 (2003).

63. Vitousek, P. M., Porder, S., Houlton, B. Z. & Chadwick, O. A. Terrestrial phosphorus limitation: mechanisms, implications, and nitrogen–phosphorus interactions. *Ecol. Appl.* **20**, 5–15 (2010).

64. Lovett, G. M. et al. Nutrient retention during ecosystem succession: a revised conceptual model. *Front. Ecol. Environ.* **16**, 532–538 (2018).

65. Du, E. et al. Global patterns of terrestrial nitrogen and phosphorus limitation. *Nat. Geosci.* **13**, 221–226 (2020).

66. Camarero, L. & Catalan, J. Atmospheric phosphorus deposition may cause lakes to revert from phosphorus limitation back to nitrogen limitation. *Nat. Commun.* **3**, 1118 (2012).

67. Elser, J. J. et al. Shifts in lake N:P stoichiometry and nutrient limitation driven by atmospheric nitrogen deposition. *Science* **326**, 835–837 (2009).

68. Hansen, H. P. & Koroleff, F. Determination of nutrients. in *Methods of Seawater Analysis* (eds. Grasshoff, K., Kremling, K., Ehrhardt, M.) 159–228 (John Wiley & Sons, Ltd, 1999).

69. Global Modeling And Assimilation Office & Pawson, S. *MERRA-2 inst3_3d_aer_Nv: 3d,3-Hourly,Instantaneous,Model-Level,Assimilation,Aerosol Mixing Ratio V5.12.4*. <https://catalog.data.gov/dataset/> (2015).

70. Barkjohn, K. K., Gantt, B. & Clements, A. L. Development and application of a United States-wide correction for PM_{2.5} data collected with the PurpleAir sensor. *Atmos. Meas. Tech.* **14**, 4617–4637 (2021).

71. Nash, J. E. & Sutcliffe, J. V. River flow forecasting through conceptual models part I—A discussion of principles. *J. Hydrol.* **10**, 282–290 (1970).

72. Petroff, A. & Zhang, L. Development and validation of a size-resolved particle dry deposition scheme for application in aerosol transport models. *Geosci. Model Dev.* **3**, 753–769 (2010).

73. Dewitz, J. *National Land Cover Database (NLCD) 2021 Products*. U.S. <https://data.usgs.gov> (2023).

74. Schroeder, W., Oliva, P., Giglio, L. & Csiszar, I. A. The New VIIRS 375 m active fire detection data product: algorithm description and initial assessment. *Remote Sens. Environ.* **143**, 85–96 (2014).

75. NASA VIIRS Land Science Team. *VIIRS/JPSS2 Active Fires 6-Min L2 Swath 375m NRT*. <https://www.earthdata.nasa.gov/> (2024).

76. Earth Science Data Systems, N. *VJ114/IMGTDL_NRT | Earthdata*. <https://www.earthdata.nasa.gov/learn/find-data/near-real-time/firms/vj114imgtdlnrt> (2020).

77. Virtanen, P. et al. SciPy 1.0: fundamental algorithms for scientific computing in Python. *Nat. Methods* **17**, 261–272 (2020).

Acknowledgements

The research provided in this paper was supported by the Cornell University Botanic Gardens. Z.G. was supported through the NSF supported CorGGLE (Cornell University GeoPaths Geoscience Learning Ecosystem) undergraduate research program (NSF-RISE-2119927). We thank G. Scheibler, E. Negron-Alvarez, J. Wang, K. Russo, S. Kolodny, and E. Johnson for their efforts in sample and data collection. We also extend our gratitude to N. Mahowald for sharing expertise on smoke aerosol dry deposition dynamics and L. Derry for thoughtful comments and conversations. We acknowledge the use of data and/or imagery from NASA's Fire Information for Resource Management System (FIRMS) (<https://earthdata.nasa.gov/firms>), part of NASA's Earth Science Data and Information System (ESDIS).

Author contributions

N.M.F. designed the study and conceptualization, analyzed main results, visualization, and writing of the paper. H.T.J. led meteorological and aerosol concentration data compilation along with HYSPLIT aerosol particle tracking results. H.T.J. and Z.G. collected and generated data and contributed to method development under the supervision of N.M.F. All authors contributed to manuscript reviewing and editing.

Competing interests

The authors declare no competing interests.

Additional information

Supplementary information The online version contains supplementary material available at <https://doi.org/10.1038/s43247-024-01732-w>.

Correspondence and requests for materials should be addressed to Nicole M. Fernandez.

Peer review information *Communications Earth & Environment* thanks the anonymous reviewers for their contribution to the peer review of this work. Primary Handling Editors: Yongqiang Liu, Somaparna Ghosh, Martina Grecequet, Heike Langenberg. A peer review file is available.

Reprints and permissions information is available at <http://www.nature.com/reprints>

Publisher's note Springer Nature remains neutral with regard to jurisdictional claims in published maps and institutional affiliations.

Open Access This article is licensed under a Creative Commons Attribution 4.0 International License, which permits use, sharing, adaptation, distribution and reproduction in any medium or format, as long as you give appropriate credit to the original author(s) and the source, provide a link to the Creative Commons licence, and indicate if changes were made. The images or other third party material in this article are included in the article's Creative Commons licence, unless indicated otherwise in a credit line to the material. If material is not included in the article's Creative Commons licence and your intended use is not permitted by statutory regulation or exceeds the permitted use, you will need to obtain permission directly from the copyright holder. To view a copy of this licence, visit <http://creativecommons.org/licenses/by/4.0/>.

© The Author(s) 2024